Available online at www.sciencedirect.com
ScienceDirect
Sensors and Actuators A 144 (2008) 231–241
SENSORS AND ACTUATORS A PHYSICAL
www.elsevier.com/locate/sna

Integrated IPMC/PVDF sensory actuator and its validation in feedback control

Zheng Chen, Ki-Yong Kwon, Xiaobo Tan *

Smart Microsystems Laboratory, Department of Electrical & Computer Engineering, Michigan State University, East Lansing, MI 48824, USA

Received 10 November 2007; received in revised form 22 January 2008; accepted 27 January 2008
Available online 19 February 2008

Abstract

Position and/or force feedback is critical in ensuring precise and safe operation of ionic polymer–metal composite (IPMC) actuators in bio/micromanipulation. In this paper the design of an integrated sensory actuator is presented, where polyvinylidene fluoride (PVDF) films are used to provide simultaneous feedback of bending and force outputs of the IPMC actuator. The design adopts differential configurations for sensing, which eliminates corruption of sensing signals by feedthrough of actuation signal or by thermal drift. Experimental results are presented to demonstrate closed-loop control of IPMC bending output based upon the integrated PVDF sensor, together with simultaneous tip force measurement with μN resolution.

Keywords: Ionic polymer–metal composite (IPMC); Polyvinylidene fluoride (PVDF); Sensory actuator; Integrated sensory feedback

1. Introduction

IPMCs form an important category of electroactive polymers (also known as artificial muscles) and have built-in actuation and sensing capabilities [1,2]. An IPMC sample typically consists of a thin ion-exchange membrane (e.g., Nafion), chemically plated on both surfaces with a noble metal as electrode [3]. When a voltage is applied across an IPMC, transport of hydrated cations and water molecules within the membrane and the associated electrostatic interactions lead to bending motions, and hence the actuation effect. Because of their softness, resilience, biocompatibility and the capability of producing large deformation under a low action voltage, IPMCs are very attractive materials for many emerging applications in biomedical devices [4–8], biomimetic robots [9–12], and micro/nano-manipulation [13–17].

In various aforementioned applications for IPMC actuators, feedback or monitoring of actuator bending and/or force outputs is often desirable and even necessary. Take microinjection of Drosophila embryos [16,18]. The path of the microinjector needs to be precisely controlled to inject genetic substance into the right spot inside the embryo; in the mean time, the injection force needs to be monitored closely to prevent rupture of embryo membrane. Existing studies on feedback control of IPMC actuators have typically adopted bulky, external sensors, such as laser vibrometers [19,20], laser distance sensors [21–23], and load cells [21]. However, it is usually unrealistic to use large, separate sensors in intended micro-and bio-applications of IPMCs due to size and safe concerns. Therefore, there is a pressing need for compact, integrated sensing technologies in order to fully realize the potential of IPMC actuators.

There have been a number of attempts to develop integrated sensors for IPMC actuators. One intriguing idea would be to use an IPMC simultaneously as actuator and sensor, like the self-sensing scheme proposed for piezoelectric materials [24]. However, this approach is difficult to implement due to the very weak sensing signal compared to the actuation signal (millivolts versus volts) [1] and the nonlinear [25], dynamic [26,2] sensing responses. Punning *et al.* proposed an integrated sensing strategy by exploiting the correlation between IPMC surface electrode resistance and the bending curvature [27,28]. This method relies on the assumption that the behavior of IPMC surface resistance is constant, which is often not true as the resistance varies with time

* Corresponding author. Tel.: +1 517 4325671; fax: +1 517 3531980.
E-mail addresses: chenzhe1@egr.msu.edu (Z. Chen), kwonki3@msu.edu (K.-Y. Kwon), xbtan@msu.edu (X. Tan).

0924-4247/$ – see front matter © 2008 Elsevier B.V. All rights reserved.
doi:10.1016/j.sna.2008.01.023

and environmental conditions (temperature, humidity, pH and salinity). Newbury [29] explored the idea of using two IPMCs, mechanically coupled in a side-by-side or bilayer configuration, to perform actuation and sensing. The attempt was unsuccessful since the sensing signal was buried in the feedthrough signal from actuation [29].

In our earlier work an integrated sensing scheme was proposed by bonding a polyvinylidene fluoride (PVDF) film to an IPMC actuator [16]. While preliminary studies showed that the approach was promising, several factors hinder it from being useful in practical feedback control. First, the capacitive coupling between IPMC and PVDF layers induces a fictitious sensing signal due to direct feedthrough of the actuation signal. Although it is possible to remove the feedthrough component through model-based compensation, this significantly increases the processing complexity; furthermore, the coupling behavior could vary over time. The second problem is due to the thermal sensitivity of PVDF – temperature variation in the environment leads to substantial drift of the PVDF sensing output, making it unusable for bending feedback. Note that PVDF was also used in fabrication of sensorized polypyrrole actuator by Ryu *et al.* [30]. Although the authors did not discuss it, the feedthrough coupling problem was also present; see Fig. 4 in [30], where spikes in the sensor output were due to abrupt changes of the actuation signal, as analyzed in [16]. No feedback control was demonstrated either in [30].

The major contribution of this paper is a new design of IPMC/PVDF sensory actuator which eliminates aforementioned problems and enables feedback control in applications. The key idea is to adopt a differential configuration for PVDF sensors. Two PVDF films are bonded to an IPMC actuator in a sandwich fashion, and a differential charge sensing circuit is used to measure the sensor output. As analyzed and verified experimentally later in the paper, this design has a number of advantages: (1) it allows shielding of capacitive coupling between IPMC and PVDF, and eliminates fictitious, feedthrough sensing signal induced directly by the actuation signal; (2) it removes the influence of thermal fluctuation and other environmental noises, which is often the most challenging problem for PVDF sensors; (3) it compensates for asymmetric sensing responses of a single PVDF film under compression versus extension; and (4) it minimizes the internal stress at bonding interfaces, which could otherwise cause delamination of layers or spontaneous creep of the composite beam structure. A second contribution of this paper is the design of an IPMC actuator with both bending and force feedback. A force sensor with μN resolution is designed by sandwiching a relatively rigid beam with two PVDF films. The force sensor is then bonded to the tip of the IPMC actuator (which itself is sandwiched by PVDF for sensing of bending).

The effectiveness of the proposed sensory actuator has been demonstrated in feedback control experiments. Precise position tracking of the end-effector is achieved through proportional-integral (PI) control based upon feedback from the integrated sensor. A laser distance sensor is used as an independent observer for validation purposes. The capability of simultaneous force measurement is shown in experiments of piercing soap bubbles. Interaction forces as low as μN are well captured.

The remainder of the paper is organized as follows. The design of IPMC/PVDF structure is described in Section 2. Robustness of the proposed design is characterized and demonstrated experimentally in Section 3. Experimental results on feedback control are presented in Section 4. Finally, concluding remarks are provided in Section 5.

2. Design of IPMC/PVDF sensory actuator

2.1. Integrated sensor for bending output

Fig. 1 illustrates the design of the integrated bending sensor for an IPMC actuator. Two complementary PVDF films, placed in opposite poling directions, are bonded to both sides of an IPMC with insulating layers in between. In our experiments, we have used 30 μm thick PVDF film from Measurement Specialties Inc., and 200 μm thick IPMC from Environmental Robots Inc. The IPMC uses non-water-based solvent and thus operates consistently in air, without the need for hydration. Scrapbooking tape (double-sided adhesive tape, 70 μm thick) from 3M Scotch Ltd., is used for both insulating and bonding purposes. A picture of a prototype is shown at the bottom of Fig. 1. Since we are focused on demonstrating the proof of the concept in this paper, the materials used are chosen mainly based on convenience. However, the models to be presented later will allow one to optimize the geometry design and material choice based on applications at hand.

The differential charge amplifier, shown in Fig. 2, is used to measure the PVDF sensor output. In particular, the inner sides of two PVDF films are connected to the common ground, while the outer sides are fed to the amplifiers. Let $Q_1(s)$ and $Q_2(s)$ be the charges generated on the upper PVDF and the lower PVDF, respectively, represented in the Laplace domain. The signals V_p^+ and V_p^- in Fig. 2 are related to the charges by

$$V_p^+(s) = -\frac{R_1 s}{1 + R_1 C_1 s} Q_1(s), \quad V_p^-(s) = -\frac{R_1 s}{1 + R_1 C_1 s} Q_2(s),$$

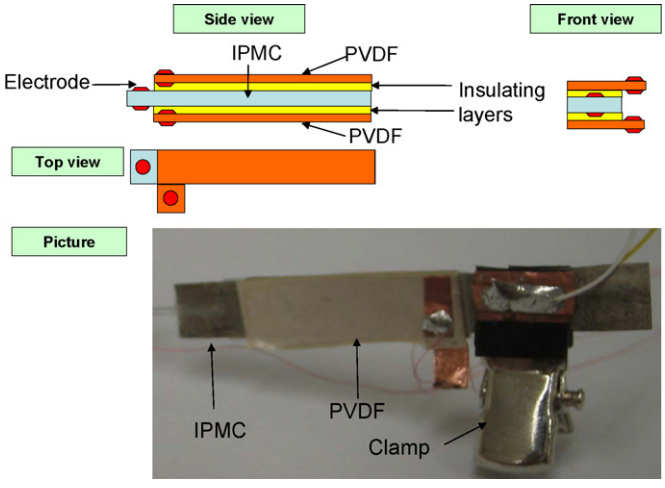

Fig. 1. Design of the IPMC/PVDF composite structure for sensing of bending output (force sensor not shown).

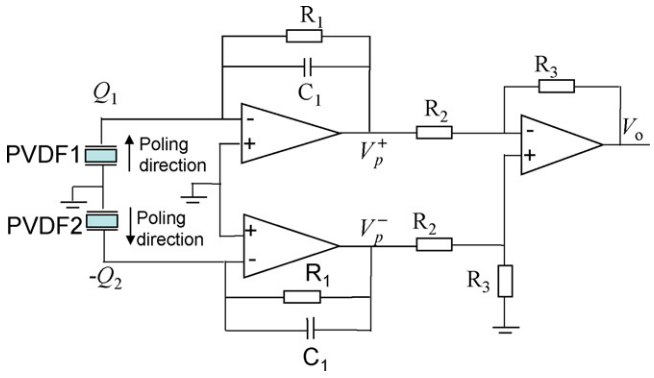

Fig. 2. Differential charge amplifier for PVDF sensor.

and the sensor output V_0 equals

$$V_0(s) = \frac{R_1 R_3 s}{R_2(1 + R_1 C_1 s)}(Q_1(s) - Q_2(s)). \tag{1}$$

Let the bending-induced charge be $Q(s)$ for the upper PVDF, and the common noise-induced charge be $Q_n(s)$. If the sensor response is symmetric under compression versus tension (more discussion on this in Section 3.3), one has $Q_1(s) = Q(s) + Q_n(s)$, $Q_2(s) = -Q(s) + Q_n(s)$, which implies

$$V_0(s) = \frac{2R_1 R_3 s}{R_2(1 + R_1 C_1 s)} Q(s), \tag{2}$$

and the effect of common noises (such as thermal drift and electromagnetic interference) is eliminated from the output. The charge amplifier (2) is a high-pass filter. To accommodate the actuation bandwidth of IPMC (typically below 10 Hz), the R_1 and C_1 values in the circuit are properly chosen so that the cutoff frequency of the charge amplifier is sufficiently low. By picking $R_1 = 5000\,\mathrm{M\Omega}$, $C_1 = 1350$ pF and $R_2 = R_3 = 10\,\mathrm{k\Omega}$, a cutoff frequency of 0.023 Hz is achieved.

A model is developed for predicting the sensitivity of the bending sensor in terms of the design geometry and material properties. Refer to Fig. 3 for the definition of geometric variables. Suppose that the IPMC/PVDF beam has a small uniform bending curvature with tip displacement z_1; without external

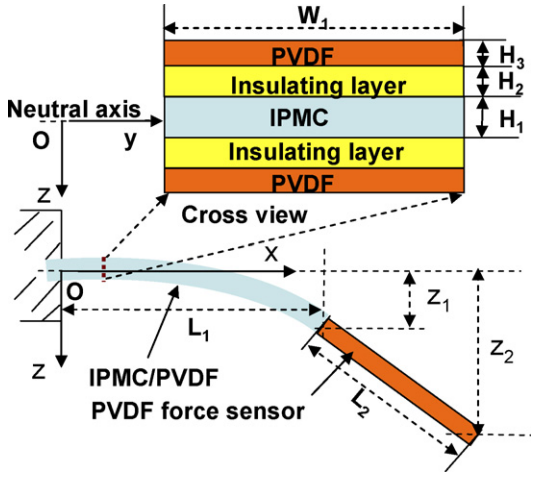

Fig. 3. Geometric definitions of IPMC/PVDF sensory actuator.

force, the force sensor beam attached at the end of IPMC/PVDF appears straight with tip displacement z_2. One would like to compute the sensitivity Q/z_2, where Q represents charges generated in one PVDF layer given the end-effector displacement z_2. With the assumption of small bending for IPMC/PVDF beam, the curvature can be approximated by [31]

$$\frac{1}{\rho} \approx \frac{2z_1}{L_1^2}, \tag{3}$$

where ρ represents the radius of curvature. As $H_3 \ll 0.5H_1 + H_2$, we assume the stress inside the PVDF to be uniform and approximate it by the value at the center line of this layer:

$$\sigma_s = E_3 \epsilon = E_3 \frac{0.5H_1 + H_2 + 0.5H_3}{\rho}, \tag{4}$$

where E_3 is the Young's modulus of the PVDF. The electric displacement on the surface of PVDF is

$$D_s = d_{31}\sigma_s, \tag{5}$$

where d_{31} is the transverse piezoelectric coefficient. The total charge generated on the PVDF is then

$$Q = \int D_s \,\mathrm{d}S = D_s L_1 W_1. \tag{6}$$

With (3)–(6), one can get

$$Q = \frac{2d_{31}E_3 W_1(0.5H_1 + H_2 + 0.5H_3)z_1}{L_1}. \tag{7}$$

The end-effector displacement z_2 is related to z_1 by

$$z_2 = z_1 + L_2 \sin\left(\arctan\left(\frac{2z_1}{L_1}\right)\right) \approx z_1\left(1 + \frac{2L_2}{L_1}\right). \tag{8}$$

Combining (7) and (8), one can get the sensitivity

$$S = \frac{Q}{z_2} = \frac{2d_{31}E_3 W_1(0.5H_1 + H_2 + 0.5H_3)}{L_1 + 2L_2}. \tag{9}$$

Table 1 lists the parameters measured or identified for our prototype. The sensitivity is predicted to be 1830 pC/mm, while the actual sensitivity is characterized to be 1910 pC/mm using a laser distance sensor (OADM 20I6441/S14F, Baumer Electric). With the charge amplifier incorporated, the sensitivity (V_0/z_2) at frequencies of a few Hz or higher is measured to be 2.75 V/mm, compared to a theoretical value of 2.71 V/mm.

Table 1
Parameters identified for the IPMC/PVDF sensory actuator prototype (including force sensor)

W_1	L_1	H_1	H_2	H_3
10 mm	40 mm	200 μm	65 μm	30 μm
W_2	L_2	h_1	h_2	h_3
6 mm	30 mm	200 μm	65 μm	30 μm
E_1	E_2	E_3	d_{31}	
5 GPa	0.4 GPa	2 GPa	28 pC/N	

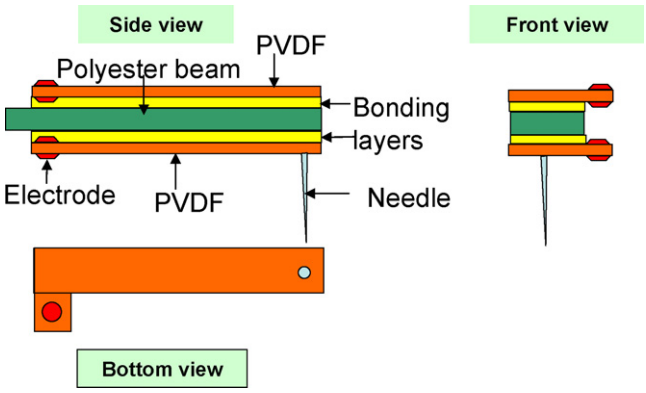

Fig. 4. Design of the force sensor for the end-effector.

2.2. Force sensor for end-effector

The structure of the force sensor is similar to that of IPMC/PVDF sensory actuator. As illustrated in Fig. 4, two PVDF films are bonded to the both sides of a relatively rigid beam. In our experiments, we have used 200 μm thick polyester from Bryce Corp., for the beam. An end-effector, e.g., a glass needle in microinjection applications, is bonded to the tip of the force sensor. An external force experienced by the end-effector will cause the composite beam to bend, which produces charges on the PVDF films. Another differential charge amplifier as in Fig. 2 is used for the force sensor. The whole force-sensing beam is attached to the front end of the IPMC/PVDF beam.

Refer to Fig. 5. The sensitivity model for force sensing, Q_f/F, is provided below. Here Q_f represents the charges generated in one PVDF in response to the force F exerted by the end-effector. The beam curvature can be written as

$$\frac{1}{\rho(x)} = \frac{F(L_2 - x)}{\sum_{i=0}^{3} E_i I_i}, \tag{10}$$

where $\rho(x)$ denotes the radius of curvature at x, E_1, E_2, E_3 are the Young's moduli of the polyester film, the bonding layer, and PVDF, respectively. I_1, I_2 and I_3 are the moments of inertia for those layers, which are given by

$$I_1 = \frac{1}{12} W_2 h_1^3,$$

$$I_2 = \frac{1}{6} W_2 h_2^3 + \frac{W_2 h_2 (h_1 + h_2)^2}{2},$$

$$I_3 = \frac{1}{6} W_2 h_3^3 + \frac{W_2 h_3 (h_1 + 2h_2 + h_3)^2}{2}.$$

The stress generated in the PVDF is approximately

$$\sigma_3(x) = E_3 \epsilon_3(x) = E_3 \frac{h_1 + 2h_2 + h_3}{2\rho(x)}. \tag{11}$$

With (5), (10) and (11), one can get the electric displacement in PVDF,

$$D_3(x) = d_{31}\sigma_3(x) = E_3 d_{31} \frac{h_1 + 2h_2 + h_3}{2} \frac{F(L_2 - x)}{\sum_{i=0}^{3} E_i I_i}. \tag{12}$$

The total charge generated in the PVDF can be written as

$$Q_f = \int_0^{L_2} D_3(x) W_2 \, dx = \frac{d_{31} E_3 W_2 L_2^2 (h_1 + 2h_2 + h_3)}{4\sum_{i=0}^{3} E_i I_i} F. \tag{13}$$

Then the sensitivity of the force sensor is

$$S_f = \frac{Q_f}{F} = \frac{d_{31} E_3 W_2 L_2^2 (h_1 + 2h_2 + h_3)}{4\sum_{i=0}^{3} E_i I_i}. \tag{14}$$

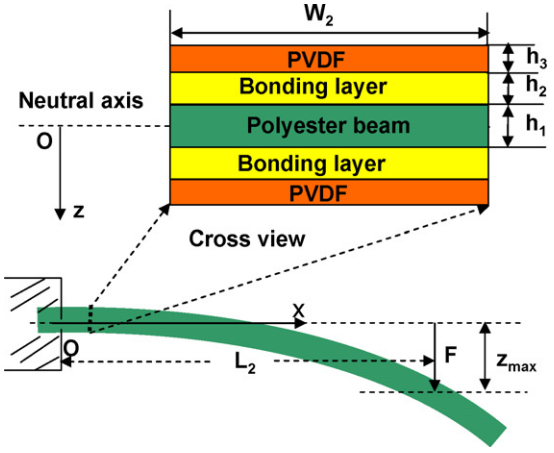

Fig. 5. Geometric definitions of the PVDF sensor.

Relevant parameters for the force sensor in our prototype can be found in Table 1. Theoretical value of S_f is computed to be 0.456 pC/ μN, which is close to the actual value 0.459 pC/ μN from measurement. With the charge amplifier circuit, the sensitivity of the overall force sensor V_{0f}/F at high frequencies (several Hz and above) is characterized to be 0.68 mV/ μN, compared to the model prediction of 0.67 mV/ μN.

The integrated IPMC/PVDF sensory actuator and the charge sensing circuits are placed in conductive plastic enclosures (Hammond Manufacturing) to shield electromagnetic interference (EMI) and reduce air disturbance and thermal drift. A slit is created on the side of the shielding box enclosing IPMC/PVDF so that the end-effector protrudes out for manipulation purposes. Fig. 6 shows the picture of the overall system.

3. Experimental verification of sensor robustness

In this section we experimentally verify the robustness of the proposed sensory actuator with respect to the following undesirable factors: (1) feedthrough of actuation signal, (2) thermal drift and other environmental noises, and (3) asymmetric PVDF sensing responses during compression versus tension. The discussion will be focused on the PVDF sensor for IPMC bending output, since the problems associated with the PVDF force sen-

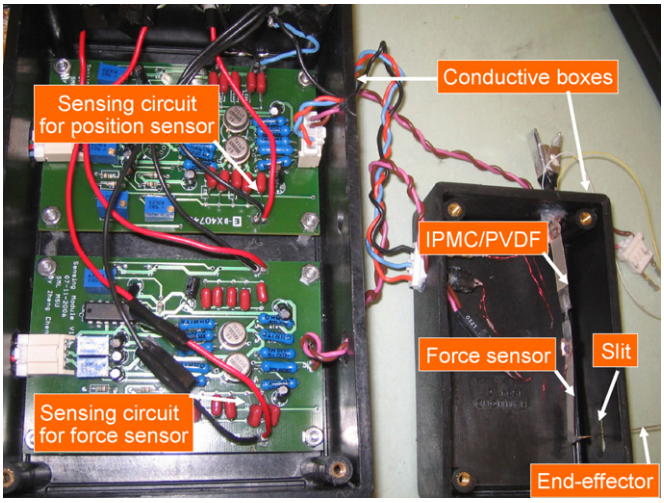

Fig. 6. IPMC/PVDF sensory actuator and sensing circuits in shielding enclosures.

sor are similar and actually simpler (no need to worry about actuation feedthrough).

3.1. Feedthrough coupling

Close proximity between IPMC and PVDF results in capacitive coupling between the two. Fig. 7 illustrates the distributed circuit model for the composite IPMC/PVDF beam. Suppose that an actuation signal $V_i(s)$ is applied to IPMC. If one connects both sides of a single PVDF film to a differential charge amplifier, as done typically [16], the output will pick up a signal that is induced by the actuation signal via electrical coupling. This feedthrough effect distorts the bending-induced charge output. Fig. 8, reproduced from [16], illustrates the traditional feedthrough problem: as a square-wave actuation signal is applied, PVDF sensor output shows spikes when actuation voltage jumps, while such spikes are not observed in actual bending. While one can attempt to model the feedthrough coupling and cancel it through feedforward compensation [16], the complexity of such algorithms and the varying behavior of coupling make this approach unappealing to real applications.

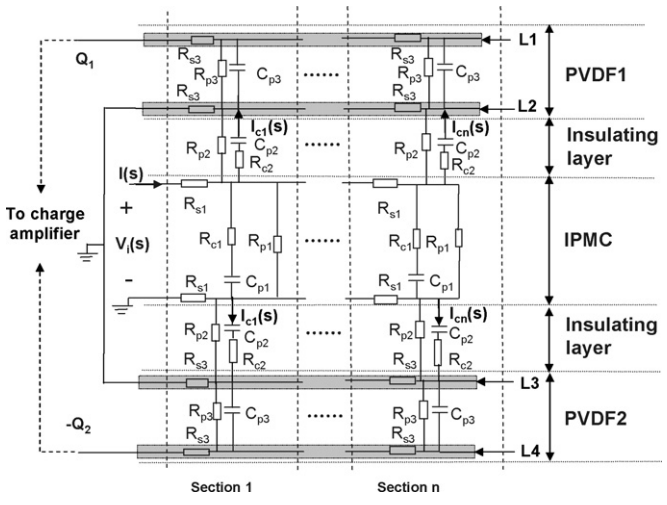

Fig. 7. Distributed circuit model of IPMC/PVDF beam.

In the new charge sensing scheme proposed in this paper, the inner sides of the two PVDF sensors are connected to a common ground (see Fig. 2). Since the surface electrode resistances of PVDF films are very low (<0.1 Ω), the inner layers L_2 and L_3 in Fig. 7 will effectively play a shielding role and eliminate the feedthrough coupling signals. This analysis is verified experimentally, where a square-wave actuation voltage with amplitude 2 V and frequency 0.1 Hz is applied to the IPMC. Fig. 9(a) shows that the charge amplifier output V_0 contains no feedthrough-induced spikes. The definitions for V_0, V_p^+, and V_p^- in the figure can be found in Fig. 2. Furthermore, the bending displacement obtained from the PVDF output V_0 correlates well with the actual bending displacement measured by the laser distance sensor, as shown in Fig. 9(b). Note that the PVDF output V_0 is related to the bending displacement z_1 through the charge amplifier dynamics (2) and the proportional relationship (7). Since (2) represents a high-pass filter, at relatively high frequencies (determined by the cut-off frequency), the correlation between V_0 and z_1 can be approximated by a constant; however, at lower frequencies (including the step input, in particular), the dynamics (2) has to be accommodated to obtain the displacement trajectory from the raw PVDF signal V_0. The latter has been adopted throughout the paper, whether the inverse of the charge amplifier dynamics is implemented digitally to retrieve z_1.

3.2. Thermal drift and environmental noises

PVDF sensors are very sensitive to ambient temperatures and electromagnetic noises. Such environmental noises could significantly limit the use of PVDF bending/force sensors, especially when the operation frequency is low (comparing with the fluctuation of ambient conditions). Refer to Fig. 2. Let noise-induced charges be Q_{n_1} and Q_{n_2} for PVDF1 and PVDF2, respectively. Suppose that no actuation signal is applied, and thus bending-induced charge $Q(s) = 0$. The voltage signals can then be expressed as

$$V_p^+(s) = -\frac{R_1 s}{1 + R_1 C_1 s} Q_{n_1}(s), \tag{15}$$

$$V_p^-(s) = -\frac{R_1 s}{1 + R_1 C_1 s} Q_{n_2}(s), \tag{16}$$

$$V_0(s) = \frac{R_1 R_3 s}{R_2(1 + R_1 C_1 s)} (Q_{n_1}(s) - Q_{n_2}(s)). \tag{17}$$

Inside a conductive shielding enclosure, thermal and EMI conditions are relatively steady and uniform. This implies $Q_{n_1}(s) \approx Q_{n_2}(s)$ and the influence of environmental noises on the sensor output V_0 is negligible.

Two experiments have been conducted to confirm the above analysis. In order to isolate the effect of noises, no actuation signal is applied. In the first experiment, the IPMC/PVDF beam was exposed to ambient air flows and electromagnetic noises. Fig. 10(a) shows the complementary sensing outputs V_p^+ and V_p^- and the resulting charge amplifier output V_0. From (15)–(17),

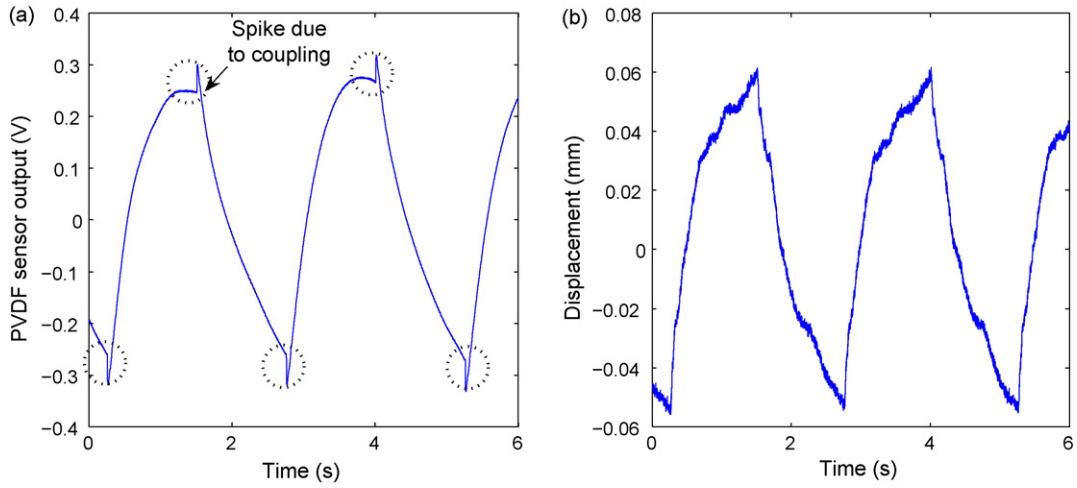

Fig. 8. Illustration of feedthrough coupling problem [16]. (a) Sensing output from the PVDF, showing the spikes from electrical feedthrough; (b) actual bending displacement detected by a laser distance sensor, showing no spikes.

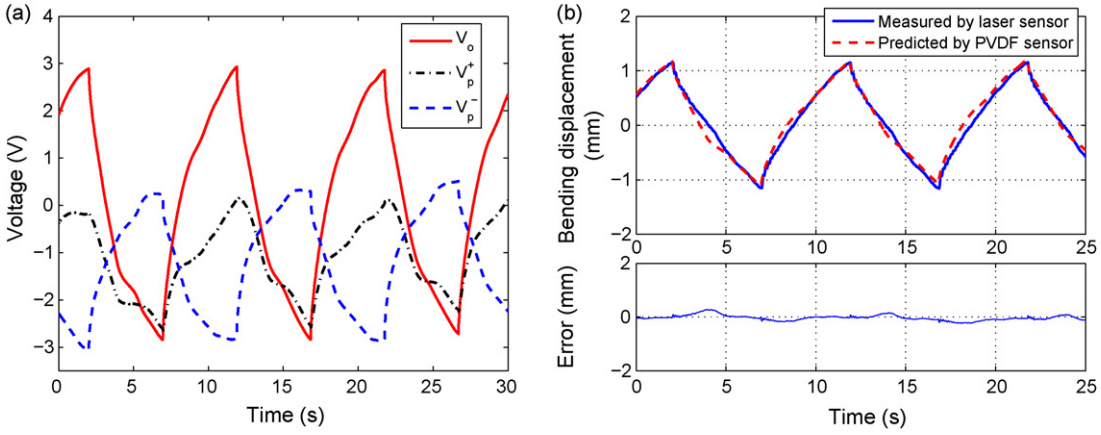

Fig. 9. Experimental results showing elimination of feedthrough signal. (a) Raw PVDF sensing signals under a square-wave actuation input (2 V, 0.1 Hz); (b) comparison between the bending displacements obtained from the PVDF sensor and from the laser sensor.

the discrepancy between V_p^+ and V_p^- indicates that the noise-induced charges Q_{n_1} and Q_{n_2} on the two PVDF layers can be significantly different, leading to relatively large sensing noise in V_0. In contrast, Fig. 10(b) shows the results from the second experiment, where the IPMC/PVDF sensory actuator was placed inside the conductive shielding enclosure. In this case, while V_p^+ and V_p^- could still vary over time individually, their trajectories are highly correlated and close to each other. Consequently, V_0 remained under 1 mV, compared to about 20 mV in the first case. These experiments have confirmed that the pro-

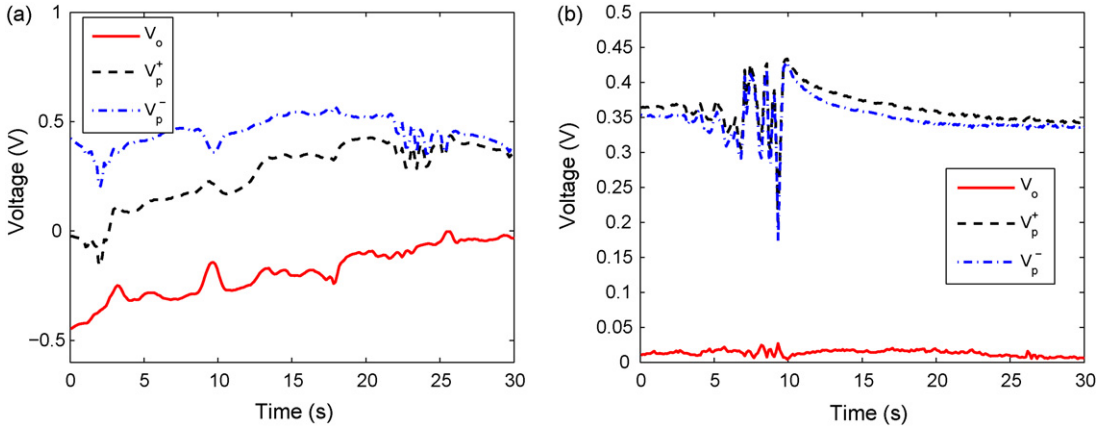

Fig. 10. (a) Sensing noise when IPMC/PVDF placed in open field; (b) sensing noise when IPMC/PVDF placed inside conductive shielding enclosure.

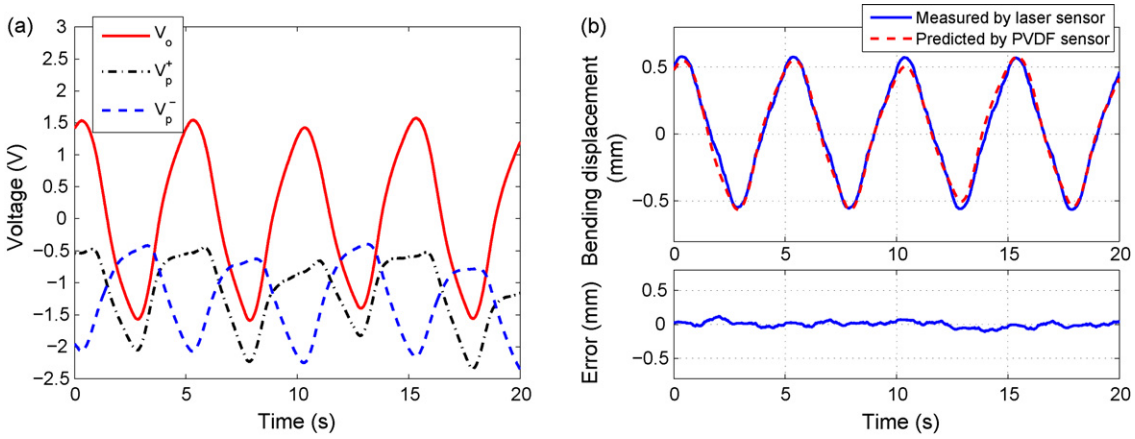

Fig. 11. Self-compensation of asymmetric tension/compression sensing response. (a) Raw PVDF sensing signals under a sinusoidal actuation signal (0.2 Hz, amplitude 1 V); (b) comparison between the bending displacements obtained from the PVDF sensor and from the laser sensor.

posed differential sensing scheme, together with the shielding enclosure, can effectively minimize the effect of thermal drift and other common noises.

3.3. Asymmetric sensing response during extension versus compression

Because of its compliant nature, a single PVDF film does not produce symmetric charge responses when it is under tension versus compression. In particular, it is difficult to effectively introduce compressive normal stress into the flexible film. As a result, the charge response of a PVDF layer under extension can faithfully capture the beam motion while the response under compression cannot. This is illustrated by experimental results shown in Fig. 11(a): each of the sensing signals V_p^+ and V_p^- from the two PVDF layers is asymmetric under a symmetric, sinusoidal actuation input. With the differential configuration of two PVDF films, however, the asymmetric responses of individual PVDF films combine to form a symmetric output V_0, as seen in Fig. 11(a). This is because when one film is in compression, the other is in tension. Fig. 11(b) shows that the bending displacement obtained based on the PVDF signal V_0 agrees well with the laser sensor measurement. We have further examined the performance of the proposed integrated sensing scheme under other types of actuation inputs, including the step inputs. From Fig. 12, the bending trajectory under a step input (2 V) can be captured well by the PVDF sensor.

Another advantage of adopting two complementary PVDF films is that it alleviates the effect of internal stresses at bonding interfaces. When bonding a single PVDF to IPMC, mismatch of internal stresses at the PVDF/IPMC interface could lead to delamination and/or spontaneous creep of the composite beam. While this problem could be lessened by using appropriate bonding technologies, it was found that the proposed scheme can effectively maintain the structural stability of the composite beam, without stringent requirements on bonding.

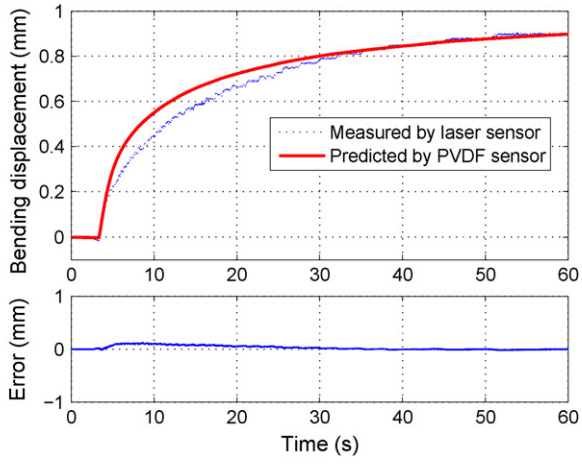

Fig. 12. Comparison between the bending displacements obtained from the PVDF sensor and from the laser sensor, when a 2 V step input is applied.

4. Feedback control based on integrated sensor

The practical utility of the proposed IPMC/PVDF sensory actuator has been demonstrated in feedback control experiments. Trajectory tracking experiments are first performed, where no tip interaction force is introduced. Simultaneous trajectory tracking and force measurement are then conducted to examine both integrated bending and force sensors.

4.1. Feedback control of bending displacement

Fig. 13 illustrates the closed-loop system for the control of IPMC bending displacement. Here $P(s)$ represents the actuation dynamics for the IPMC/PVDF composite structure, $H(s)$ is the bending sensor dynamics, $K(s)$ is the

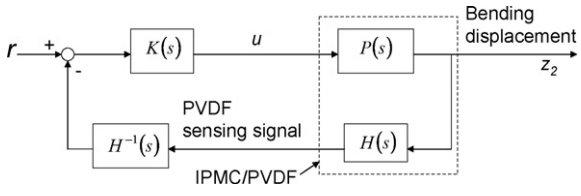

Fig. 13. Closed-loop system for control of IPMC bending displacement.

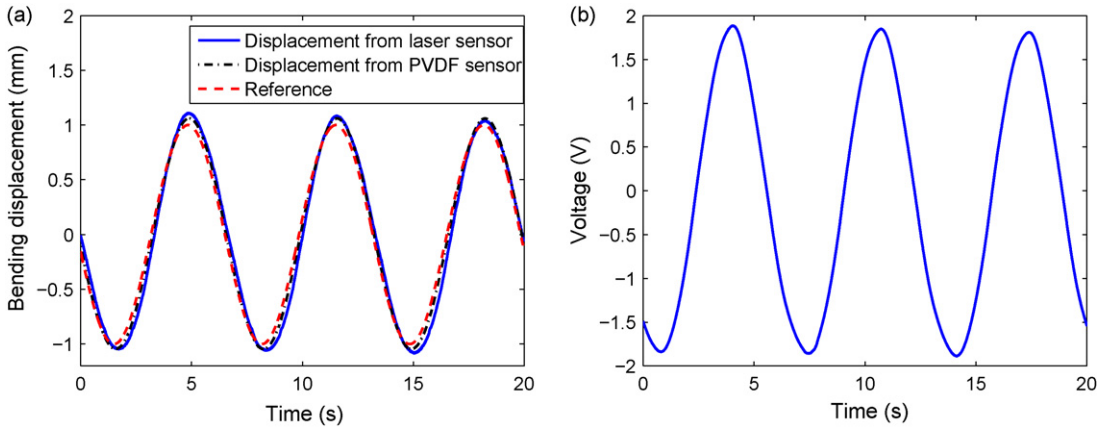

Fig. 14. Experimental results on feedback control of bending displacement using integrated PVDF sensor. (a) Bending displacement; (b) actuation voltage.

controller, r is the reference input, u is the actuation voltage, and z_2 is the bending displacement of the end-effector. In experiments data acquisition and control calculation are performed by a dSPACE system (DS1104, dSPACE Inc.); for real applications such tasks can be easily processed by embedded processors, e.g., microcontrollers. A laser sensor is used as an external, independent observer for verification purposes.

In general $K(s)$ can be designed based on a nominal model of the plant $P(s)$ and various objectives and constraints. An example of H_∞ control design can be found in [23], where a physics-based, control-oriented model is also developed for IPMC actuators. Since IPMC modeling and control design are not the focus of this paper, we have identified the plant model $P(s)$ empirically and used a simple proportional-integral (PI) controller for $K(s)$ to validate the integrated sensing scheme. In particular, the empirical frequency response of the IPMC/PVDF sensory actuator has been obtained by applying a sequence of sinusoidal actuation inputs (amplitude 0.2 V, frequency 0.01–10 Hz) and measuring the corresponding bending response. It has been found that the measured dynamic behavior could be approximated by a second-order system, the parameters of which have been further determined using the Matlab command "fitsys". The resulting $P(s)$ is

$$P(s) = \frac{2.7s + 20}{1000(s^2 + 33.4s + 18.9)}. \tag{18}$$

The sensing model is obtained from (2) and (7):

$$H(s) = \frac{18150s}{6.57s + 1}. \tag{19}$$

The following reference trajectory is used: $r(t) = \sin(0.3\pi t)$ mm. Based on the models and the reference, a PI controller $K(s) = 1000(40 + (30/s))$ is designed to achieve good tracking performance while meeting the constraint $|u| < 2$ V. Fig. 14(a) shows the experimental results of tracking the bending reference. It can be seen that the PVDF sensor output tracks the reference well; furthermore, the actual bending displacement, as observed by the laser sensor, has close agreement with the PVDF output. The actuation voltage u, shown in Fig. 14(b), falls within the limit $[-2, 2]$ V.

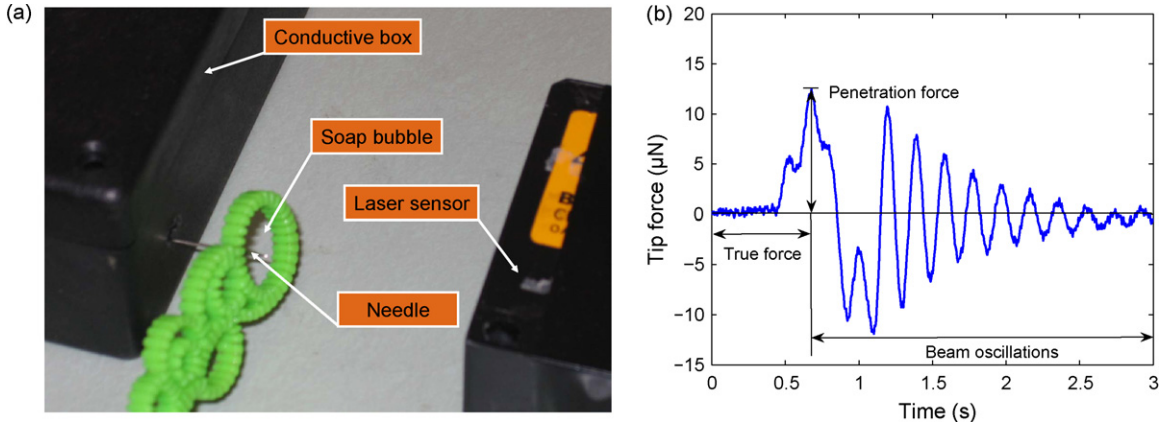

Fig. 15. Measurement of the micro-force in piercing soap bubbles. (a) Experimental setup; (b) PVDF sensor response during and after penetration.

4.2. Feedback bending control with simultaneous force measurement

It is desirable in many applications to have both displacement and force feedback. With the proposed IPMC/PVDF sensory actuator, one can perform feedback control of the displacement while monitoring the force output, as well as perform feedback control of the force output while monitoring the displacement. In the following experiment we will demonstrate the feedback bending control with simultaneous force measurement.

To mimic the force level often encountered in bio and micromanipulation applications, we have attached a sharp glass needle as an end-effector at the tip of force-sensing beam and used it to pierce soap bubbles. Fig. 15(a) shows the experimental setup. A number of bubble-penetrating experiments were conducted to get an estimate of the rupture force by moving a bubble manually towards the needle until it breaks, when no actuation voltage was applied. Fig. 15(b) shows the force sensor response during a typical run. It can be seen that the response first rises from zero to a peak value, and then starts decayed oscillations. Since the PVDF sensor measures essentially the bending of the passive beam, its output can be interpreted as an interaction force only when the end-effector is in contact with a foreign object. Thus for the response in Fig. 15(b), only the first rising segment truly represents the force, after which the membrane ruptures and the beam starts oscillating. Hence we take the peak value of such responses as the penetration force. Fig. 16 shows the penetration force measured in 26 independent experiments. Overall the measurements are consistent with an average of 11 μN. The variation is believed due to the randomly created bubbles that might have different thicknesses. Note that for many real applications, such as microinjection of embryos or cells [16], the end-effector will maintain contact with the object under manipulation, in which case the output of PVDF force sensor would truly represent the interaction force at all times.

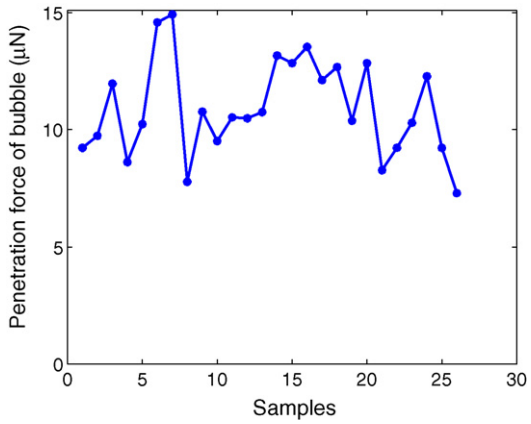

Fig. 16. Measured forces during penetration of soap bubble membranes.

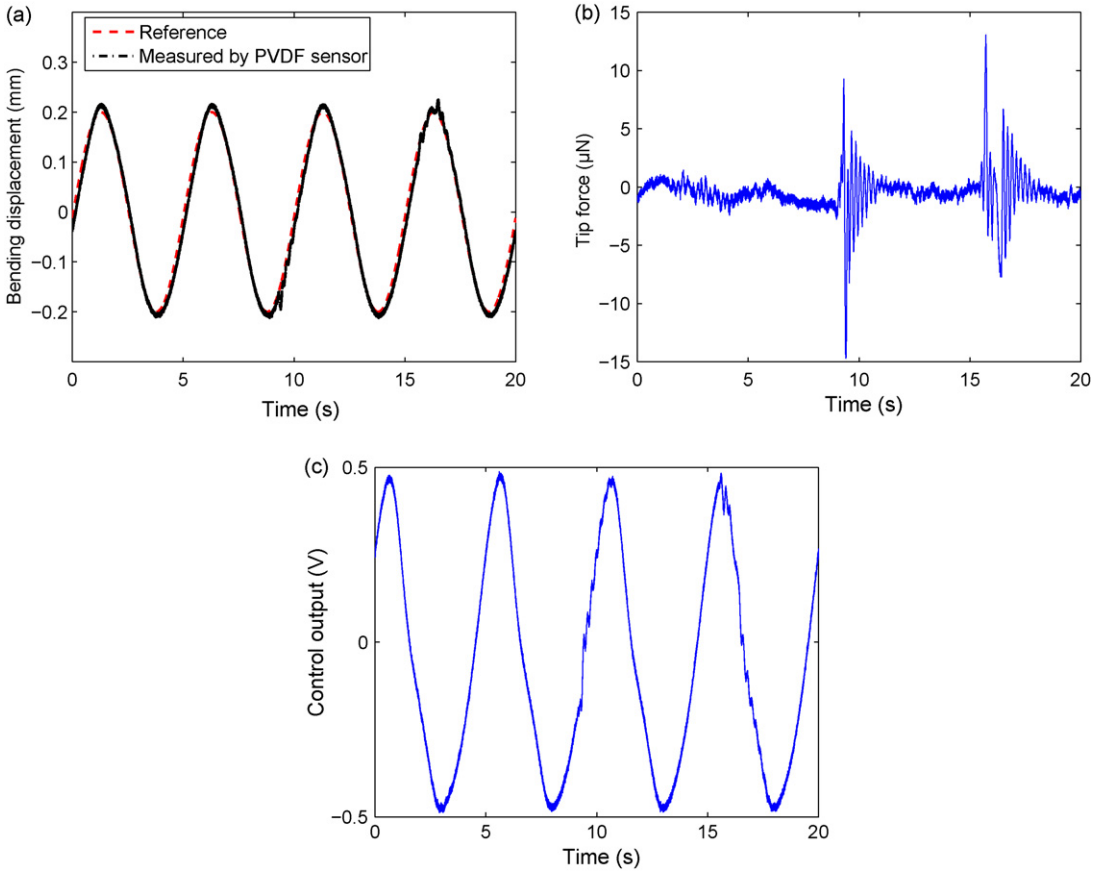

Fig. 17. Experimental results on bending feedback control with tip force measurement. (a) Displacement of the end-effector estimated based on the integrated PVDF bending sensor alone; (b) PVDF force sensor output; (c) actuation voltage generated by the feedback controller.

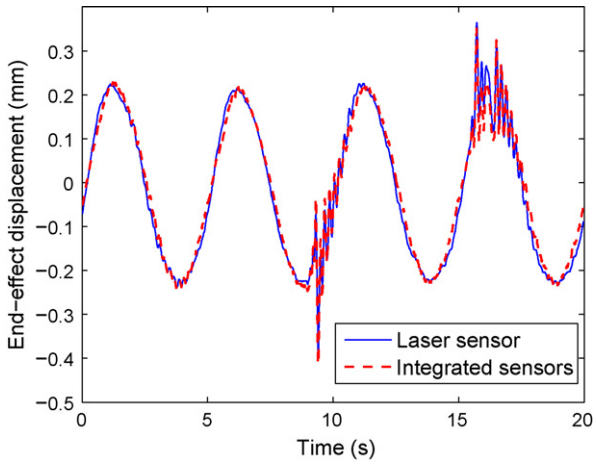

Fig. 18. Estimation of true end-effector displacement by combining the integrated bending and force sensors, and its comparison with the laser sensor measurement.

A feedback bending control experiment with force monitoring has been conducted, where the reference for the end-effector displacement $r(t) = 0.2\sin(0.4\pi t)$mm. During the experiment, the end-effector penetrated two soap bubbles at $t = 9.32$ s and $t = 15.72$ s, respectively. Fig. 17(a) shows the estimated end-effector displacement based on the integrated PVDF bending sensor (sandwiching IPMC), under the assumption that the force-sensing PVDF beam is not deflected. The estimated displacement trajectory follows closely the reference, with slight perturbations at the moments when penetrations occur, indicating that the feedback control was in effect. Fig. 17(b) shows the output of the integrated force sensor, where the two penetrations were captured clearly. Note that, as explained earlier and illustrated in Fig. 15(b), only the first rising segment of the trajectory during each penetration truly represents the interaction force, while the remaining portion of the signal arises from oscillations following penetration. The control output (actuation voltage) is shown in Fig. 17(c), where one can see that feedback is in action to suppress the disturbance caused by penetration.

Note that the end-effector displacement z_2 predicted by the PVDF bending sensor alone (Fig. 17(a)) does not capture the true displacement d when the end-effector interacts with objects. To obtain the true displacement, one can combine the bending sensor output z_2 and the force sensor output F:

$$d = z_2 + \frac{F}{k}, \tag{20}$$

where k is the stiffness of the force-sensing beam. For our prototype, $k = 0.067$ N/m. Fig. 18 compares the end-effector displacement obtained from (20) and that observed by the laser sensor, which shows that indeed the end-effector position can be monitored by combining the integrated bending and force sensors.

5. Conclusions and future work

In this paper a novel scheme was proposed for implementing integrated sensors for an IPMC actuator, to achieve sensing of both the bending displacement output and the force output. In the design two thin PVDF films are bonded to both sides of an IPMC beam to measure the bending output, while a passive beam sandwiched by two PVDF films is attached at the end of IPMC actuator to measure the force experienced by the end-effector. The differential configuration adopted in both sensors has proven critical in eliminating feedthrough coupling, rejecting sensing noises induced by thermal drift and EMI, compensating asymmetric tension/compression responses, and maintaining structural stability of the composite beams. For the first time, feedback control of IPMC was successfully demonstrated using only integrated sensors, showing that one can simultaneously regulating/tracking the bending displacement and monitoring the force output (or vice versa).

In the interest of clarity, we adopted an assumption of small deformation for IPMC actuators in model derivation throughout this paper. This allowed us to represent the bending state of an IPMC actuator with its tip displacement. The presented sensitivity models, (9) and (14), were also based on this assumption. However, such an assumption has its limitations for many IPMC applications where the deformation is relatively large. The discrepancies between the bending displacements obtained from PVDF and from the laser sensor, as shown in Figs. 9, 11 and 12, could be an example of such limitations. In future work, it is important to extend the models to accommodate large bending motions by incorporating nonlinear elasticity theory for composite beams.

This work brings IPMC materials much closer to their envisioned applications in bio-and micro-manipulation, robotics, and biomedical systems, where position and/or force outputs need to be closely controlled or monitored. Future work includes applying the developed IPMC/PVDF sensory actuator to such applications, one of which is precision control of microinjection of Drosophila embryos [18].

Acknowledgements

This research was supported in part by an NSF CAREER grant (ECS 0547131) and MSU IRGP (05-IRGP-418). The authors wish to thank Dr. Yantao Shen for his help in calibration of the PVDF force sensor.

References

[1] M. Shahinpoor, K.J. Kim, Ionic polymer–metal composites: I. Fundamentals, Smart Mater. Struct. 10 (2001) 819–833.
[2] Z. Chen, X. Tan, A. Will, C. Ziel, A dynamic model for ionic polymer–metal composite sensors, Smart Mater. Struct. 16 (2007) 1477–1488.
[3] K.J. Kim, M. Shahinpoor, Ionic polymer–metal composites: II. Manufacturing techniques, Smart Mater. Struct. 12 (2003) 65–79.
[4] S. Guo, T. Fukuda, K. Kosuge, F. Arai, M. Negoro, Micro-catheter system with active guide wire, in: Proceedings of IEEE International Conference on Robotics and Automation, 1995, pp. 79–84.
[5] M. Shahinpoor, K. Kim, Ionic polymer–metal composites: IV. Industrial and medical applications, Smart Mater. Struct. 14 (2005) 197–214.
[6] G.-H. Feng, R.-H. Chen, Fabrication and characterization of arbitrary shaped μIPMC transducers for accurately controlled biomedical applications, Sens. Actuators A: Phys. 143 (2008) 34–40.

[7] B.-K. Fang, M.-S. Ju, C.-C.K. Lin, A new approach to develop ionic polymer–metal composites (IPMC) actuator: fabrication and control for active catheter systems, Sens. Actuators A: Phys. 137 (2007) 321–329.
[8] W.J. Yoon, P.G. Reinhall, E.J. Seibel, Analysis of electro-active polymer bending: a component in a low cost ultrathin scanning endoscope, Sens. Actuators A: Phys. 133 (2007) 506–517.
[9] S. Guo, T. Fukuda, K. Asaka, A new type of fish-like underwater microrobot, IEEE/ASME Trans. Mechatron. 8 (1) (2003) 136–141.
[10] B. Kim, J. Ryu, Y. Jeong, Y. Tak, B. Kim, J.-O. Park, A ciliary based 8-legged walking micro-robot using cast IPMC actuators, in: Proceedings of IEEE International Conference on Robots and Automation, 2003, pp. 2940–2945.
[11] B. Kim, D.-H. Kim, J. Jung, J.-O. Park, A biomimetic undulatory tadpole robot using ionic polymer–metal composite actuators, Smart Mater. Struct. 14 (2005) 1579–1585.
[12] X. Tan, D. Kim, N. Usher, D. Laboy, J. Jackson, A. Kapetanovic, J. Rapai, B. Sabadus, X. Zhou, An autonomous robotic fish for mobile sensing, in: Proceedings of the IEEE/RSJ International Conference on Intelligent Robots and Systems, Beijing, China, 2006, pp. 5424–5429.
[13] J.W.L. Zhou, H.-Y. Chan, T.K.H. To, K.W.C. Lai, W.J. Li, Polymer MEMS actuators for underwater micromanipulation, IEEE/ASME Trans. Mechatron. 9 (2) (2004) 334–342.
[14] S. Tadokoro, S. Yamagami, M. Ozawa, Soft micromanipulation device with multiple degrees of freedom consisting of high polymer gel actuators, in: Proceedings of IEEE International Conference on Micro-Electro Mechanical Systems, 1999, pp. 37–42.
[15] R. Lumia, M. Shahinpoor, Microgripper design using electroactive polymers, in: Smart Structures and Materials 1999: Electroactive Polymer Actuators and Devices, 1999, pp. 322–329.
[16] Z. Chen, Y. Shen, N. Xi, X. Tan, Integrated sensing for ionic polymer–metal composite actuators using PVDF thin films, Smart Mater. Struct. 16 (2007) S262–S271.
[17] T. Nguyen, N. Goo, V. Nguyen, Y. Yoo, S. Park, Design, fabrication, and experimental characterization of a flap valve IPMC micropump with a flexibly supported diaphragm, Sens. Actuators A 141 (2008) 640–648.
[18] Y. Shen, U.C. Wejinya, N. Xi, C.A. Pomeroy, Force measurement and mechanical characterization of living Drosophila embryos for human medecal study, J. Eng. Med. 221 (2) (2007) 99–112.
[19] K. Mallavarapu, D. Leo, Feedback control of the bending response of ionic polymer actuators, J. Intell. Mater. Syst. Struct. 12 (2001) 143–155.
[20] C. Kothera, Characterization, Modeling and Control of the Nonlinear Actuation Response of Ionic Polymer Transducers, Virginia Polytechnic Institute and State University, Blacksburg, Virginia, 2005.
[21] N. D. Bhat, Modeling and precision control of ionic polymer metal composite, Master's thesis, Texas A&M University, 2003.
[22] R.C. Richardson, M.C. Levesley, M.D. Brown, J.A. Hawkes, K. Watterson, P.G. Walker, Control of ionic polymer metal composites, IEEE/ASME Trans. Mechatron. 8 (2) (2003) 245–253.
[23] Z. Chen, X. Tan, A control-oriented, physics-based model for ionic polymer–metal composite actuators, in: Proceedings of the 46th IEEE Conference on Decision and Control, New Orleans, LA, 2007, pp. 590–595.
[24] J. Dosch, D. Inman, E. Garcia, A self-sensing piezoelectric actuator for collocated control, J. Intell. Mater. Syst. Struct. 3 (1992) 166–185.
[25] C. Bonomo, C.D. Negro, L. Fortuna, S. Graziani, D. Mazza, Characterization of IPMC strip sensorial properties: preliminary results, in: Proceedings of International Symposium on Circuits and Systems, 2003, pp. IV-816–IV-819.
[26] K. Farinholt, D. Leo, Modeling of electromechanical charge sensing in ionic polymer transducers, Mech. Mater. 36 (2004) 421–433.
[27] A. Punning, M. Kruusmaa, A. Aabloo, Surface resistance experiments with IPMC sensors and actuators, Sens. Actuators A 133 (2007) 200–209.
[28] A. Punning, M. Kruusmaa, A. Aabloo, A self-sensing ion conducting polymer metal composite (IPMC) actuator, Sens. Actuators A 136 (2007) 656–664.
[29] K. M. Newbury, Characterization, modeling, and control of ionic polymer transducers, Ph.D. thesis, Virginia Polytechnic Institute and State University, 2002.
[30] J. Ryu, J. Park, B. Kim, J.-O. Park, Design and fabrication of a largely deformable sensorized polymer actuator, Biosens. Bioelectron. 21 (2005) 822–826.
[31] Z. Chen, X. Tan, M. Shahinpoor, Quasi-static positioning of ionic polymer–metal composite (IPMC) actuators, in: Proceedings of the IEEE/ASME International Conference on Advanced Intelligent Mechatronics, Monterey, CA, 2005, pp. 60–65.

Biographies

Zheng Chen received his BS degree in Electrical Engineering and MS degree in Control Science and Engineering from Zhejiang University, China, in 1999 and 2002, respectively. He is currently pursuing his PhD degree in Electrical and Computer Engineering at Michigan State University. His research interests include modeling and control of electrical-active polymers (EAP's), EAP-based smart microsystems, control of dynamical systems with hysteresis, and neural networks.

Ki-Yong Kwon received his BS degree in Electrical Engineering from Michigan State University in 2007. He is currently a Master's student in the Department of Electrical and Computer Engineering at the same university.

Xiaobo Tan received the Bachelor's and Master's degrees in Automatic Control from Tsinghua University, Beijing, China, in 1995, 1998, and his PhD in Electrical and Computer Engineering from the University of Maryland at College Park, USA, in 2002. From September 2002 to July 2004 he was a Research Associate with the Institute for Systems Research at the University of Maryland. In August 2004 he joined the Department of Electrical and Computer Engineering at Michigan State University as an Assistant Professor. His research interests include electroactive polymer sensors and actuators, modeling and control of smart materials, biomimetic robotics, bio/micro-manipulation, and collaborative control of unmanned vehicles. Dr. Tan was a recipient of the NSF CAREER Award in 2006.